ADVANCED HEALTHCARE MATERIALS
www.advhealthmat.de

An Ultraswelling Microneedle Device for Facile and Efficient Drug Loading and Transdermal Delivery

*Zhiming Li, Puxuan Zhao, Zhixin Ling, Yanting Zheng, Fengli Qu, and Hao Chang**

The advancement and extensive demand for transdermal therapies can benefit from a safe, and efficient and user-friendly transdermal technology with broad applicability in delivering various hydrophilic drugs. Here the design and proof of concept applications of an ultraswelling microneedle device that enables the facile and efficient loading and transdermal delivery of hydrophilic drugs with different molecular weights is reported. The device consists of a super-hydrophilic hydrogel microneedle array and a resin base substrate. Using a special micromolding technique that involves hydrated crosslinking and cryogenic-demolding, the microneedle part displays a rapid swelling ratio of ≈3800%, enabling the loading of drugs up to 500 kDa in molecular weight. The drug loading process using the device just involves incubating the microneedle part in a drug solution for 1 min, followed by 15 min of drying. The microneedles can easily penetrate the skin under press and detach from the base substrate under shear, thereby releasing the payload. Administration of desired therapeutic agents using the device outperformed conventional administration methods in mitigating psoriasis and eliciting immunity. This biocompatible device, capable of withstanding ethylene oxide sterilization, can enhance the efficacy and accessibility of transdermal therapies in research institutes, hospitals, and even home settings

1. Introduction

Skin, the largest and most accessible organ of the human body, has been recognized as an extremely attractive portal for the delivery of various therapeutic agents.[1] Once administrated into the skin, drugs can either act immediately for the treatment of local dermatological disorders (e.g., psoriasis and melanoma) or permeate into the blood capillaries in the underlying dermis and then enter the systemic circulation to treat systemic diseases (e.g., diabetes and Alzheimer's disease).[2] Compared to oral delivery and parenteral injection, transdermal drug delivery offers several advantages, including a bypass of first-pass hepatic metabolism and enzymatic degradation by the gastrointestinal tract, controllable release features, and minimized systemic exposure and side effects.[3] In addition, due to the presence of abundant immune cells (Langerhans cells and dendritic cells) and lymphatic vessels in the dermal layer, the skin is also a beneficial site for vaccination with a high potential for improving the adaptive immune response.[4] However, the formidable barrier imposed by the outer stratum corneum layer of the skin significantly restricts the penetration of the large majority of drugs, especially those that are large (>500 Da) and hydrophilic molecules.[5] To reverse the low permeability of skin, various approaches have been explored to chemically or physically enhance the transport efficiency of therapeutics across the skin. Chemical penetration enhancers generally have low efficiency of large molecules and are constrained by skin irritation when using potent chemicals.[6] Physically-based methods, such as ultrasound, electroporation, iontophoresis, and thermal ablation, are often more effective; however, they can cause pain and local damage and require costly and complex equipment as well as specialized personnel, thus limiting their adoption.[7] Therefore, there is a critical need to develop a safe, simple-to-apply, and efficient transdermal delivery technology to meet the tremendous requirements of transdermal therapies.

Microneedles have been demonstrated as an advanced alternative for transdermal delivery, offering the painless and minimally invasive administration of targeted drugs into specific skin layers.[8] Drugs can be loaded into microneedles to form microneedle-based drug-device combination systems, allowing for self-administration and enhancing patient compliance.[9] Different types of microneedles have been developed using a wide range of materials and geometries, and they have successfully functioned as carriers of a variety of hydrophilic therapeutic agents ranging from small molecules (e.g., curcumin, metronidazole, and 5-fluorouracil) to large molecules (e.g., insulin, peptides, antibodies, and vaccine antigens).[9–10] These therapeutic agents are commonly loaded onto the surface of the fabricated

Z. Li, P. Zhao, Z. Ling, Y. Zheng, F. Qu, H. Chang
Hangzhou Institute of Medicine (HIM)
Chinese Academy of Sciences
Hangzhou, Zhejiang 310022, China
E-mail: changhao@ibmc.ac.cn
P. Zhao
College of Materials Science and Engineering
Zhejiang University of Technology
Hangzhou, Zhejiang 310014, China
Y. Zheng
College of Pharmaceutical Sciences
Zhejiang University of Technology
Hangzhou, Zhejiang 310014, China

The ORCID identification number(s) for the author(s) of this article can be found under https://doi.org/10.1002/adhm.202302406

DOI: 10.1002/adhm.202302406

microneedles via coating strategies, such as layer-by-layer assembly and spraying coating, or incorporated within the matrix of microneedles during the fabrication.[10b] However, these drug loading methods are complex and time-consuming, and generally involve multiple steps, which is likely to cause waste and activity loss of therapeutic agents, particularly biomacromolecules. In addition, excipient materials, formulations, and fabrication procedures have to be adjusted and optimized for preloading different drugs. From the perspective of the end users, it is impractical for those without relative expertise and equipment to load desirable drugs for research or clinical application, as compared to a syringe that allows end users to easily perform drug loading themselves. To enhance the accessibility of transdermal therapies with microneedles, there is desire to develop a microneedle platform that offers convenience and applicability in both loading and delivery of various hydrophilic drugs, ranging from small to large molecules.

In this study, we introduce an ultraswelling microneedle device (USMD) that enables the facile and efficient loading and transdermal delivery of hydrophilic drugs with different molecular weights (**Figure 1**A). The USMD consists of an array of superhydrophilic hydrogel microneedles and a resin base substrate. By using a special micromolding technique that involves hydrated crosslinking and cryogenic-demolding, the microneedle part displays a rapid swelling ratio of around 3800%, enabling the loading of drugs up to 500 kDa in molecular weight. The drug loading process using the device just involves incubating the microneedle part in a drug solution for 1 min, followed by a 15 min drying. The amount of drug loaded by USMD can be precisely controlled by regulating the drug concentration in the incubation solution. The microneedle part can easily penetrate into skin under compression and detach from the base substrate under shear as an implantable drug reservoir to release the payload. To demonstrate the clinical efficacy, the USMD was employed for loading methotrexate (MTX)/interleukin 17A antibody (IL-17A) to treat psoriasis, as well as ovalbumin (OVA) as a model antigen for immunization purposes. Administration of desired therapeutic agents using the USMD outperformed conventional administration methods (e.g., oral, topical, and injection) in mitigating psoriasis and eliciting immunity. Finally, the USMD can withstand ethylene oxide sterilization without losing its properties.

2. Results

2.1. Design, Fabrication, and Characterization of USMD

The proposed USMD is comprised of an array of ultraswelling microneedles made from crosslinked methacrylated hyaluronic acid (MeHA), and a base substrate made from a biocompatible resin. MeHA was synthesized by modifying HA with methacrylic anhydride and the degree of methacrylation was about 90% according to the ^{1}H NMR spectrum (Figure S1, Supporting Information). MeHA was chosen as the raw material for the microneedle part due to its excellent biocompatibility, which ensures the safety of the USMD.[11] Additionally, MeHA has supreme water absorbency, enabling the microneedle to rapidly absorb water and the drug molecules contained within it during the transitioning from a dry state to its maximum swelling state.[12] Unlike the previously reported hydrogel microneedle patch, where both the microneedles and base substrate were made of hydrogel materials, we utilized resin to create the base substrate of USMD. This design ensures that only the microneedle part of USMD loads drugs, thereby improving the delivery efficiency, as only the microneedle part can be embedded into the skin tissue. To fabricate the USMD, we introduced a special micromolding technique that involves hydrated crosslinking and cryogenic-demolding processes (Figure 1B). Briefly, the cavities of needles and the base substrate of the PDMS mold were filled with MeHA solution, and photocurable resin, respectively. Then, UV irradiation was applied to crosslink both the hydrated MeHA and resin. The resulting USMD was frozen at −20 °C and demolded (this step was termed cryogenic-demolding). The final USMD was obtained after complete drying at room temperature.

The hydrated crosslinking and the cryogenic-demolding are two critical steps that determine the swelling performance of USMD. Generally, the hydrogel microneedles can be crosslinked either before or after drying (hereafter referred to as "hydrated crosslinking" or "dehydrated crosslinking," respectively).[12–13] We found that the sequence of crosslinking greatly influences the swelling ability of dry MeHA hydrogel. The MeHA hydrogel with dehydrated crosslinking had a lower swelling ratio (86.37 ± 9.58%) compared to that with hydrated crosslinking (315.01% ± 8.89%). Besides, the cryogenic-demolding step could further improve the swelling ability of the USMD (Figures S2 and S3, Supporting Information). The MeHA hydrogel with hydrated crosslinking displayed a swelling ratio of 3022.61 ± 100.40% after freezing treatment, much larger than that without freezing treatment (315.01 ± 8.89%) (Table S1, Supporting Information).

Another advantage of cryogenic-demolding is that it can guarantee the reliable fabrication of the USMD. During fabrication, the USMD needs to be demolded before drying because the impermeable resin base substrate prevents the microneedle array from drying within the PDMS mold. However, the microneedle part of USMD cannot be completely peeled off from the mold after hydrated crosslinking, as evidenced by the residual rhodamine tips remaining in the mold, even with prolonged crosslinking time (Figure S4, Supporting Information). During cryogenic demolding, the frozen microneedle array could be 100% removed from the mold while keeping their structures intact. This was attributed to the improved mechanical strength resulting from ice formation, similar to demolding mechanism during the fabrication of the cryomicroneedles.[8a]

After being cryogenically demolded from the PDMS mold, the microneedle part of the USMD had its height reduced from 1800 μm (the original microneedle height of the master template) to around 600 μm during the drying process (Figure 1C; and Figure S5, Supporting Information). The crosslinking time was found to affect the swelling ability of USMD. A shorter crosslinking time resulted in larger pore size and swelling ratio of USMD (Figure 1D). The USMD crosslinked for 0.5 min (CL-0.5 min) exhibited a swelling ratio of over 6000%, while the swelling ratio of USMD crosslinked for 5 min (CL-5 min) was ≈2000% (Figure 1E; and Figure S6, Supporting Information). The swelling ability determines the drug loading capacity. We used rhodamine 6G (Rho6G, 479 Da) as a small molecular drug and fluorescein isothiocyanate-labeled ovalbumin (FITC-OVA, 40 kDa) as a macromolecular drug to conduct a preliminary assessment of the drug loading capacity of the USMD with

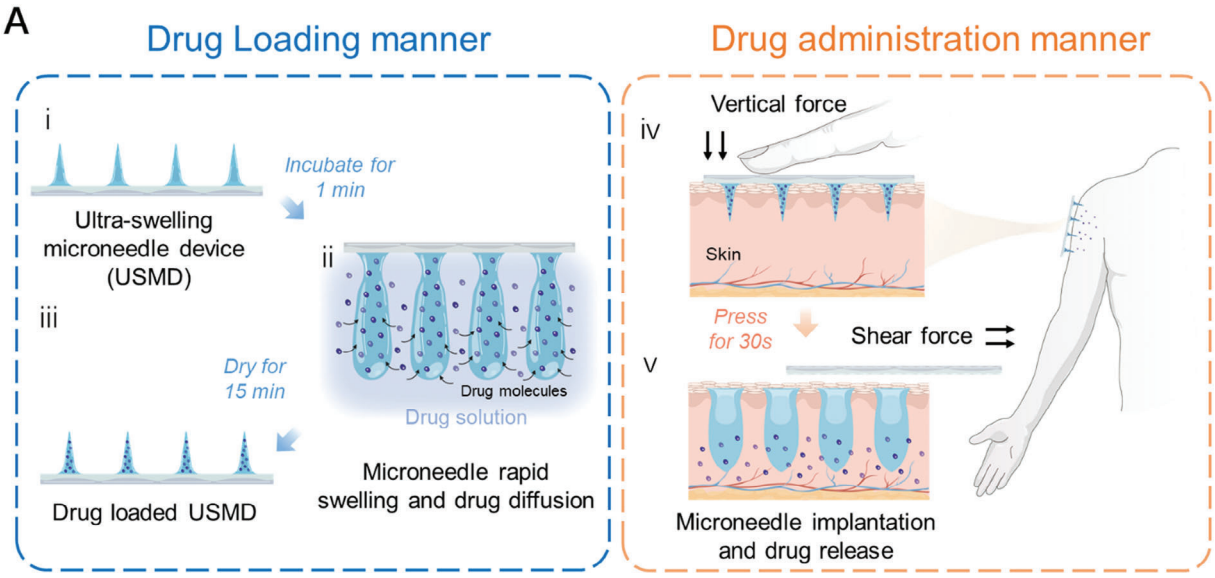

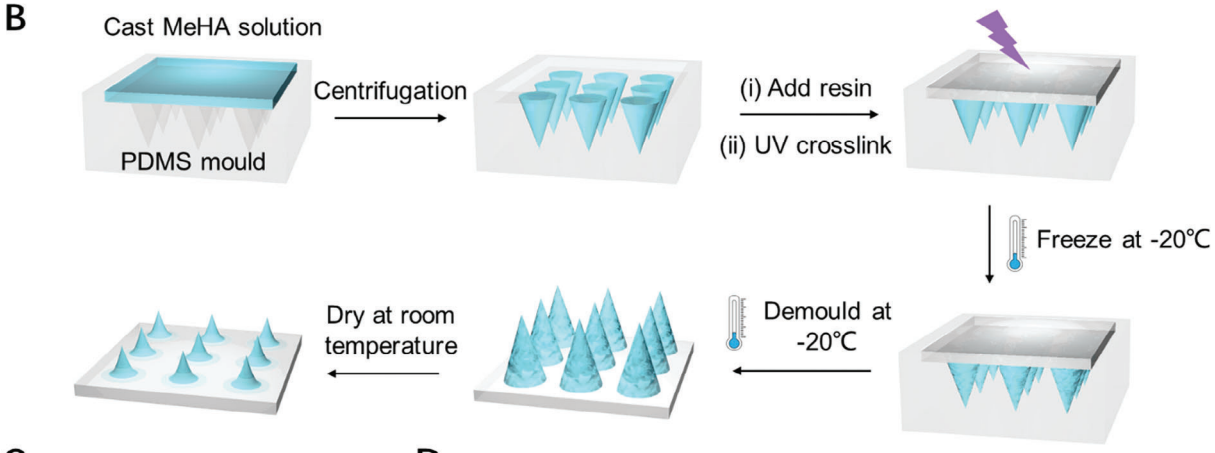

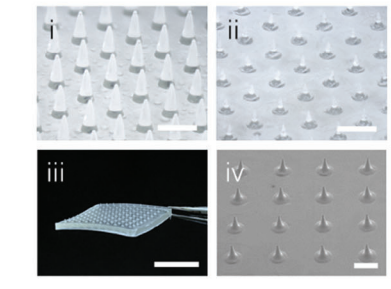

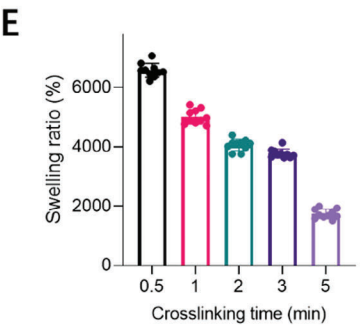

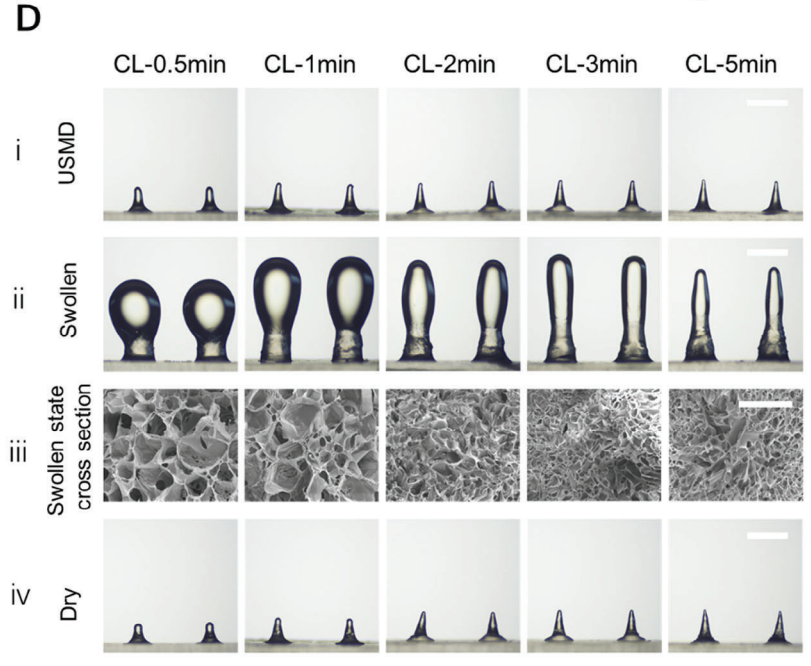

different crosslinking times (Figure S7, Supporting Information). Increasing the crosslinking time did not influence the loading capacity of small molecules but decreased the loading capacity of large molecules. However, the needle parts of USMD with lower crosslinking time could not maintain their sharp structure after drying postcryogenic-demolding and redrying postswelling. Moreover, due to insufficient crosslinking time, certain parts of the microneedles dissolved during the swelling process, as evidenced by the height variation of USMD during drug loading.

2.2. Mechanical Properties and Skin Insertion of USMD

Mechanical strength is an important factor that determines the success of inserting the USMD post drug loading into the skin tissue. To simulate the process of drug loading, the USMD with different crosslinking times were incubated in PBS to induce swelling, and then allowed to dry before conducting compression tests using a tensile testing machine. First, we needed to determine the required drying time for USMD to attain complete dryness, and recover to original morphology and optimal mechanical strength after swelling. The compressive strength was calculated by dividing the force by the cross-sectional area of USMD. We found that the compressive strength of USMD increased along with the drying time and was about 65.48 ± 4.1 MPa after 15 min drying, similar to that after 30 min drying (Figure S8, Supporting Information). The results suggest that 15 min is sufficient for USMD to completely dry at room temperature (25 °C, 40% relative humidity) after drug loading. Next, we examined the mechanical strength of USMD with different crosslinking times. The longer crosslinking time resulted in higher mechanical strength of USMD (Figure S9, Supporting Information). Specifically, the compressive strength of the USMD with crosslinking for 0.5, 1, 2, 3, and 5 min, was about 23.85 ± 3.0, 30.67 ± 4.2, 45.19 ± 4.0, 65.68 ± 4.4, and 74.28 ± 2.8 MPa, respectively (**Figure 2**A).

We also examined the skin penetration ability of USMD using porcine skin, given its recognized similarities to the anatomy of human skin.[14] As shown in Figure 2B, the skin penetration ability decreased when the USMD was crosslinked for less time because of the lower mechanical strength and the blunt structure (Figure S10, Supporting Information). Due to its sufficient mechanical strength and sharp structure, the USMD crosslinked for 3 min (CL-3 min) was able to pierce through the stratum corneum (which is about 21–26 μm thickness) with thumb force and reach the dermal layer (up to 519.3 ± 32.85 μm), similar to the USMD crosslinked for 5 min (CL-5 min) (Figure 2C). In the following experiments, we selected 3 min as the optimal crosslinking time during the fabrication of USMD, resulting in an optimal balance between drug-loading capacity and mechanical strength, while ensuring that the needles of USMD can effectively penetrate the skin.

In addition to evaluating the compressive strength of USMD, we also applied shear force to the microneedles to investigate whether they can separate from the base substrate after skin penetration. Before insertion into the skin, the USMD required the shear of 0.208 ± 0.006 N per needle to deform, and the microneedles bent without fracture. In contrast, the microneedles of USMD were easily broken after insertion into skin tissue, which was due to the decrease in mechanical properties of the microneedles after rapid swelling upon contact with the skin interstitial fluid. After insertion into the skin for 30 s, the microneedles easily separated from the base substrate under a shear force of about 0.08 N per needle (Figure 2D), which can be easily applied by finger.[15] Furthermore, we used USMD to load Rho6G and pressed USMD into porcine skin. After 30 s, gentle shear by thumb was applied to remove the base substrate of USMD. All the needles detached from the base substrate and remained embedded in the skin, as evidenced by fluorescent signals of Rho6G on the surface of the skin (Figure 2E). Images of histological sections showed that the microneedles of the USMD were fully embedded within the skin tissue after separation from the base substrate (Figure 2F).

2.3. Drug Loading Capacity of USMD

To evaluate the drug loading capacity of the USMD, we selected four types of hydrophilic molecules with different molecular weights, namely, Rho6G (479 Da), fluorescein isothiocyanate-labeled ovalbumin (FITC-OVA, 40 kDa), fluorescein isothiocyanate-labeled dextran (FITC-Dex, 150 kDa), and FITC-Dex (500 kDa) as model drugs. The microneedle part of the USMD was incubated in the drug solution, allowing the drug molecules to diffuse into the swollen microneedle matrix. Our results showed that all drug molecules could be successfully loaded inside USMD, and the amount of loading could be regulated by controlling the drug concentration in the incubation solution (**Figure 3**A; and Figures S11–S14, Supporting Information). When the concentration of drug solution is 20 mg mL^{-1}, each microneedle of the USMD was able to load 6.21 ± 0.17 μg of Rho6G, 3.70 ± 0.10 μg of FITC-OVA, 2.25 ± 0.08 μg for FITC-Dex (150 kDa), and 1.27 ± 0.12 μg for FITC-Dex (500 kDa), respectively (Figure 3B–E). Moreover, we incubated the USMD into drug solutions for different periods ranging from 10 to 300 s. We found that prolonging incubation time could increase the amount of drug loaded in the USMD. For these four types of drug molecules, the maximum amount of drug loaded in USMD was achieved after incubating USMD in the drug

Figure 1. Schematic illustration, fabrication, and characterization of USMD. A) Schematic illustration of ultraswelling microneedle device (USMD) applied manner. i), The USMD is composed of an array of ultraswelling crosslinked microneedles and the resin base substrate. ii), Ultraswelling and drug diffusion in needle matrix within 1 min. iii), USMD loaded with the drug were obtained. iv), The whole USMD needle was pressed into the skin by vertical force, and v), The base was removed by finger, and the needle part was implanted inside the skin tissue as a drug reservoir, where it gradually biodegrades and releases the drug over time. B) Schematic of USMD fabrication. C) Characterization of the USMD i), After demold at −20 °C and ii), dry at room temperature. Scale bar, 1000 μm. iii), Photographs of the USMD. Scale bar, 10 mm. iv), SEM images of the USMD. Scale bar, 1 mm. D) Drug loading simulation by PBS of USMD. i), USMD, and ii), after swelling for 1 min in PBS. Scale bar, 1000 μm. iii), SEM images of microneedle cross sections after swelling. Scale bar, 100 μm. iv), After 15 min of drying. Scale bar, 1000 μm. E) The swelling ratio of USMD with different UV crosslinking times. Data are presented as mean ± s.d. (n = 10 independent samples). In (B,C), three images were taken and all experiments were repeated independently three times with similar results.

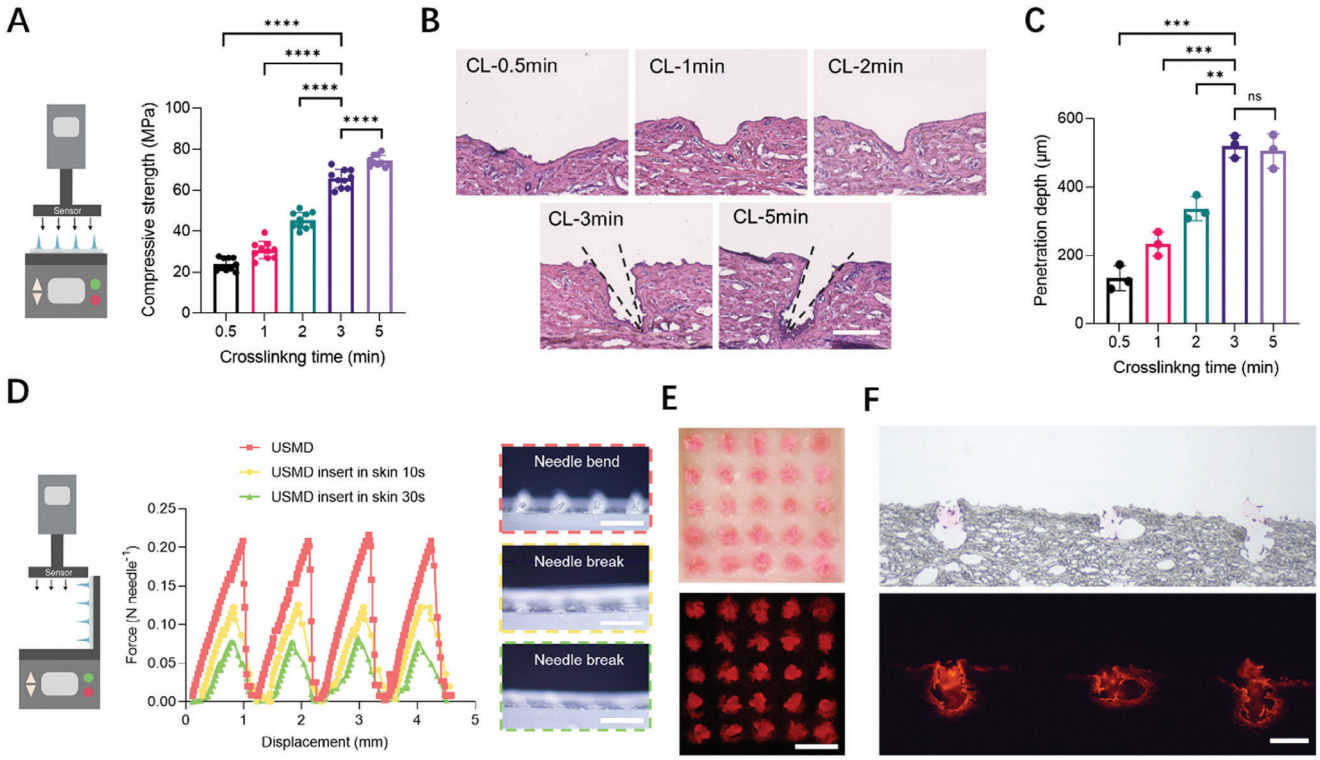

Figure 2. Mechanical properties and skin insertion of the USMD. A) The compressive strength of USMD with different crosslinking times (right) tested by an Instron tensile meter (left). Data are presented as mean ± s.d. (n = 10 independent samples). ****$P < 0.0001$ via two-sided Student's t-test. B) H&E staining images of porcine skin inserted by USMD with different crosslinking times. Scale bar, 500 μm. C) Quantitative data for the porcine skin penetration depth of USMD with different crosslinking times. Data are presented as mean ± s.d. (n = 3 independent USMD samples). Two-tailed Student's t-test was used to compare the penetration depth of USMD with different crosslinking times (***P = 0.002 vs 0.5 min; ***P = 0.005 versus 1 min; **P = 0.0028 vs 2 min; ns, P = 0.7147 vs 5 min). D) The mechanical behavior of USMD (middle graph) and insertion into the skin with 10 and 30 s under shear force (right graph) tested by an Instron Tensile Metre (left panel). Data are presented as mean ± s.d. (n = 5 independent samples). The representative bright-field microscopy images in (D) show USMD (top) and USMD after insertion in skin 10 (middle) and 30 s (bottom) after the application of shear force. Scale bar, 1000 μm. E) Representative bright-field (top) and fluorescence microscopy images (bottom) of porcine skin after USMD insertion ex vivo. Scale bar, 500 μm. F) Histological images of USMD needle embedded in porcine skin ex vivo. Bright-field (top) and fluorescence microscopy images (bottom) of representative histological sections of porcine skin after USMD loading of Rho6G, and needle insertion and separation. Scale bar, 500 μm. All experiments were repeated independently three times with similar results.

solution for 60 s (Figure S15, Supporting Information). This rapid drug loading ability was attributed to the rapid swelling ability of MeHA microneedles as reported by our previous study.[12] Besides, the height and width of USMD before incubation in the drug solution and after drying did not show significant differences (Table S2, Supporting Information). Despite there is a little increase in tip diameter, the USMD remained sharp enough to effectively penetrate the skin (Figure S24, Supporting Information). These results demonstrate the versatility and robustness of USMD in loading different types of hydrophilic drugs with varying molecular weights.

2.4. Ex Vivo and In Vivo Drug Release of USMD

To evaluate the drug-release capability of USMD when applied to the skin, we performed a release kinetics study. USMD was incubated in PBS at 37 °C to simulate physiological conditions, and the release profiles of different molecules were assessed. We found that the molecular weight of the loaded drug has a slight influence on its release from USMD. As shown in **Figure 4**A, USMD released over 90% of Rho6G (479 Da), 80% of FITC-OVA (40 kDa), 70% of FITC-Dex (150 kDa), and 60% of FITC-Dex (500 kDa) within 10 min. Rho6G (479 Da) was fully released after 20 min, whereas the larger molecules required 72 h for complete release (Figure 4B). This delayed release is due to the molecular size, which limits their mobility in the hydrogel matrix of the microneedles and the PBS solution.[16]

To predict the in vivo drug release profile, the USMD loaded with FITC-OVA (40 kDa) was embedded in a simple skin model (consisting of agarose hydrogel covered with a parafilm layer)[17] and continuously monitored under an inverted fluorescence microscope. After 0.5 min of insertion, the microneedles of the USMD rapidly swelled and easily detached from the resin base substrate, embedded in the hydrogel (Figure 4C). The microneedles reached their maximum swelling form in the hydrogel within 3 min, and FITC-OVA began to diffuse out of the needle but remained mainly located around it. After 6 h, we observed that FITC-OVA had diffused in all directions within the gel.

To further evaluate the in vivo drug release of the USMD, we monitored the fluorescence signal of FITC-OVA after its delivery into the mice's back skin using USMD (Figure 4D; and

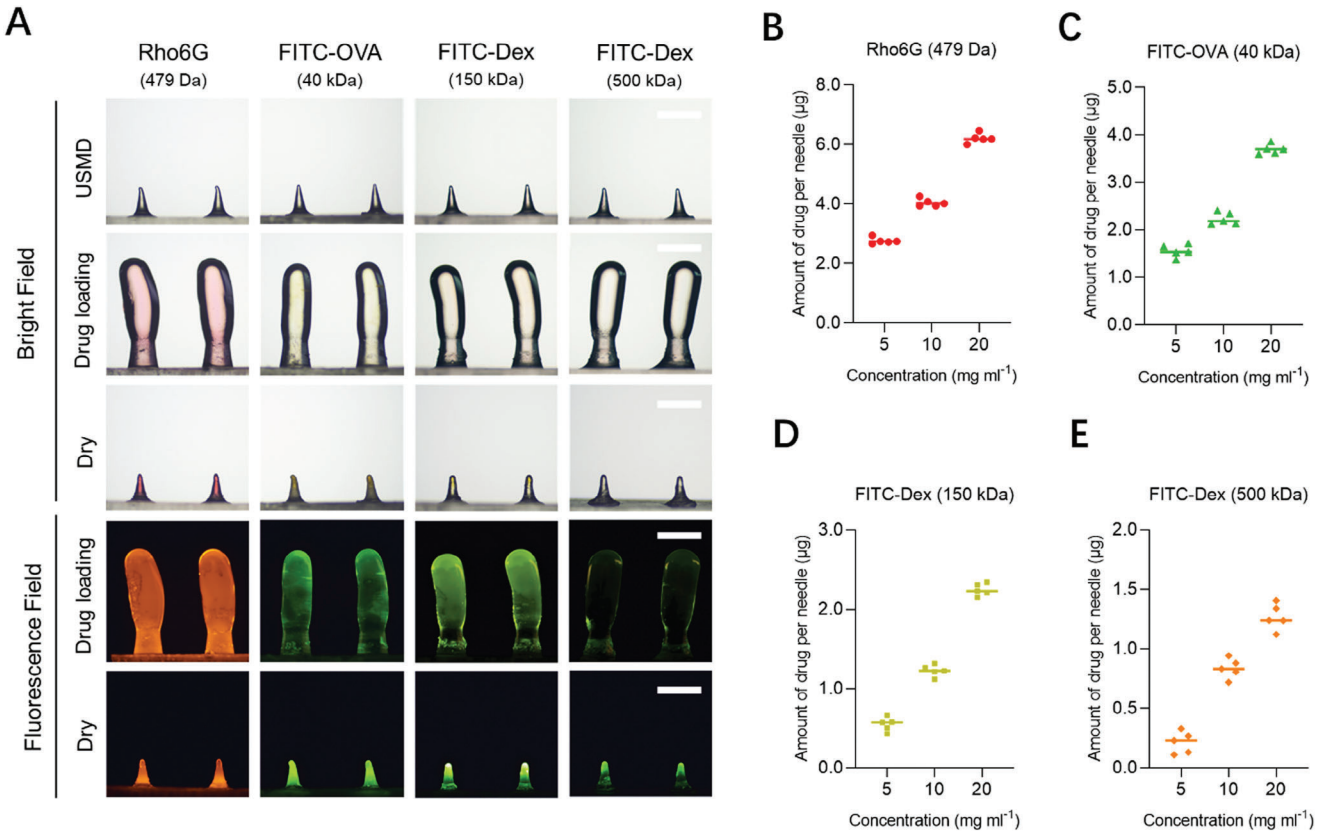

Figure 3. Drug loading capacity of the USMD. A) Representative bright-field (top) and fluorescence images (bottom) of USMD before and after the loading of Rho6G (479 Da), FITC-OVA (40 kDa), FITC-Dex (150 kDa), and FITC-Dex (500 kDa). Scale bar, 500 μm. Quantification of USMD loaded with, B) Rho6G (479 Da), C) FITC-OVA (40 kDa), D) FITC-Dex (150 kDa), and E) FITC-Dex (500 kDa) in different concentrations. Data are presented as mean ± s.d. ($n = 5$ independent samples). In (A), three images were taken and all experiments were repeated independently three times with similar results.

Figure S16, Supporting Information). A strong fluorescent signal was observed at the application site of the USMD after the microneedles were embedded into the skin, which decreased by half after 1 day. As the microneedles of USMD degraded, the signal of FITC-OVA gradually diminished and nearly disappeared within 7 days. The quantitative analysis demonstrated a consistent decrease in fluorescence intensity over time, indicating that the release of FITC-OVA from USMD was sustained for a period of 7 days (Figure 4E). The release of FITC-OVA in vivo was slower than in vitro, possibly due to the condensed extracellular matrix within the skin tissue, which slowed down the diffusion rate of FITC-OVA from the application site of USMD to the surrounding tissue.

2.5. Delivery of Therapeutics via USMD Improves the Treatment of Psoriasis

Psoriasis is a chronic autoimmune skin condition characterized by the rapid buildup of skin cells that result in red, thickened, and scaly patches on the skin.[18] Psoriasis can cause discomfort, itching, and pain, and it may also have a significant impact on a person's quality of life. Methotrexate (MTX, a small molecular drug) and interleukin 17A (IL-17A, an antibody drug) are commonly used clinically approved drugs for the treatment of psoriasis.[19] To evaluate the therapeutic potential of USMD in the treatment of psoriasis, we loaded these drugs into the USMD and administered them to mice with an imiquimod (IMQ)-induced psoriasis model. We compared the therapeutic efficacy of USMD delivery to the conventional administration methods: topical and oral administration of MTX, and subcutaneous (SC) injection of IL-17A. The administration protocols of MTX and IL-17A were illustrated in **Figure 5**A.

Repeated topical administration of IMQ on the dorsal skin of mice induced skin lesions that exhibited typical manifestations of erythema, induration, and thickening.[20] On day 7, psoriasis-like lesions were observed (Figure 5B; and Figure S17, Supporting Information), and the model group and blank USMD group exhibited severe hyperkeratosis, including epidermal hyperplasia and scaling. The treatment with MTX-loaded USMD significantly improved the severity of clinical signs and symptoms of psoriasis in the IMQ-induced skin lesions compared to conventional oral or topical therapies. Likewise, the therapeutic effect of IL-17A-loaded USMD was more significant than that of SC injection (Figure S18, Supporting Information). The severity of the disease was assessed daily using an objective scoring system, the Psoriasis Area and Severity Index (PASI) based on erythema, scaling, and induration. Based on the PASI scores, the administration of MTX and IL-17A using USMD demonstrated stronger anti-inflammatory effects compared to topical and oral delivery

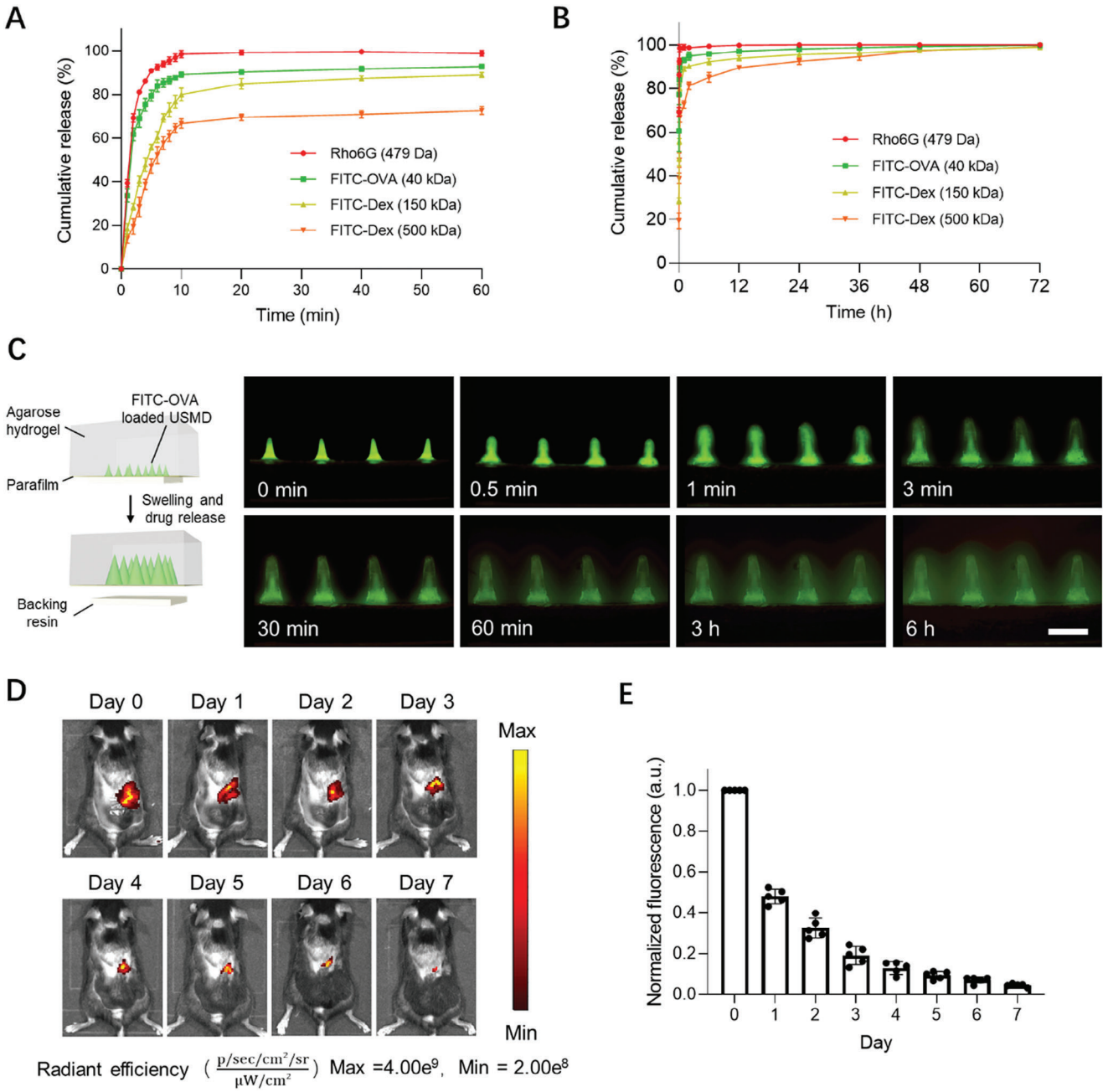

Figure 4. In vitro and in vivo drug release of USMD. A) Release profiles of Rho6G (479 Da), FITC-OVA (40 kDa), FITC-Dex (150 kDa), and FITC-Dex (500 kDa) from USMD over the first 1 h and, B) 72 h. (n = 10 independent samples). C) Time lapse of FITC-OVA diffusing from USMD needle after inserted into the skin model made of agarose hydrogel and parafilm. Scale bar, 1000 μm. D) In vivo fluorescent imaging of mice treated with USMD loaded with FITC-OVA from day 0 to 7. E) Quantification of fluorescence intensity on the skin. Data are normalized to the fluorescence intensity at day 0. Data are presented as mean ± s.d. (n = 5 independent animals). All the experiments were repeated independently three times with similar results.

of MTX, as well as subcutaneous injection of IL-17A, respectively (Figure 5C). No obvious changes in body weight and ALT levels of mice were observed during the treatment period, indicating the safety of USMD administration (Figure 5D; and Figure S19, Supporting Information). Previous reports have shown that IMQ cream can induce spleen enlargement in mice.[21] We found the spleen weight of mice treated with USMD loaded with MTX was similar to that of the control group (Figure 5E), suggesting that USMD does not cause splenomegaly. However, delivery of IL-17A using USMD did not reverse the gain of spleen weight. We speculated that antagonizing IL-17A would not modulate IMQ-induced immune cell mobilization; thus, the protective effect dependent on IL-17A is not reflected in splenomegaly.[22]

Furthermore, we used hematoxylin and eosin (H&E) staining and toluidine blue staining to examine skin tissue sections microscopically. H&E staining revealed that severe hyperkeratosis

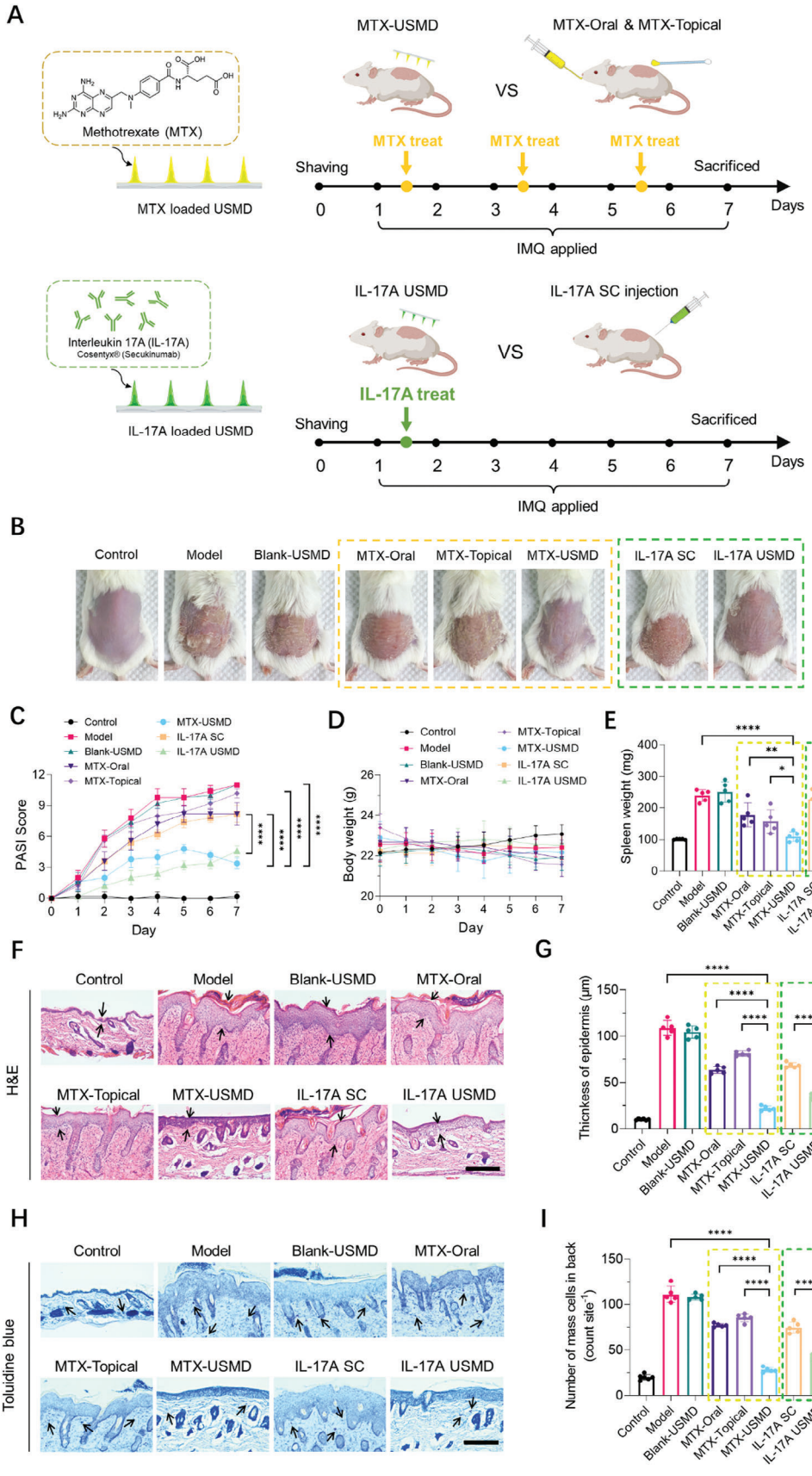

occurred in both the model group and the blank USMD group, characterized by epidermal hyperplasia and edema. The delivery of MTX and IL-17A through USMD significantly improved the IMQ-induced skin lesions in the dermis or epidermis compared to conventional delivery methods, such as oral and topical administration, as well as SC injection, respectively (Figure 5F). This was also reflected by the quantification of epidermal thickness in H&E-stained microphotographs (Figure 5G). The infiltration of mast cells into the dermis is commonly observed in psoriasis.[23] The results of toluidine blue staining on skin tissues demonstrated that the administration of MTX loaded USMD or IL-17A loaded USMD lead to a significant reduction in mast cell infiltration within the dermal layers of mouse skin, in comparison to the topical and oral administration of MTX, and the SC injection of IL-17A, respectively (Figure 5H). Mast cells are known to release various proinflammatory mediators, such as histamine and cytokines, which contribute to the pathogenesis of psoriasis.[24] The reduction in mast cell infiltration observed in our study suggests that USMD based drug delivery exhibited a stronger anti-inflammatory effect on psoriasis (Figure 5I). Collectively, these results demonstrated that administration of MTX and IL-17A using USMD could greatly improve their therapeutic efficacy in the treatment of psoriasis, compare to their conventional administration methods.

2.6. Vaccination by USMD Loaded with Antigen

To explore the potential of USMD in vaccination, we used OVA as a model vaccine antigen and loaded it into the USMD. The mice were immunized with OVA loaded USMD (OVA-USMD) three times, with each immunization administered every 5 days (**Figure 6**A). Conventional vaccination methods, including subcutaneous injection (OVA-SC) and intramuscular injection (OVA-IM), were used for comparison, with the same dosage of OVA. The levels of the surface marker CD86, and major histocompatibility complex class I (MHCI) and II (MHCII) were used to confirm the activation and maturation of DCs in the draining lymph nodes (dLNs). On day 20, dLNs were excised, and the maturation of DCs was examined based on the expression of co-stimulatory molecules, including CD11c, CD86, MHCI, and MHCII. Vaccination with OVA-USMD induced significantly higher percentages of $CD11c^+CD86^+$ DCs (1.79 ± 0.19%), $CD11c^+MHCI^+$ DCs (2.53 ± 0.18%), and $CD11c^+MHCII^+$ DCs (1.95 ± 0.26%) in the dLNs, compared with vaccination by SC (1.27 ± 0.19%, 1.85 ± 0.14%, and 1.44 ± 0.10%, respectively) and IM injection (1.06 ± 0.10%, 1.40 ± 0.12%, and 1.09 ± 0.19%) (Figure 6B–D; and Figures S20–S21, Supporting Information). The levels of OVA-specific IgG and IgG1 induced by OVA-USMD increased with each vaccination, surpassing those in the SC and IM injection groups (Figure 6E,F). Thus, OVA-USMD vaccination generates a stronger humoral immune response compared to other vaccination methods.

Furthermore, we evaluated antigen-specific cellular immunity using different vaccination methods. Compared to SC and IM injections, vaccination with OVA-USMD resulted in higher levels of OVA-specific IgG2a antibody (Figure 6G), suggesting enhanced cell-mediated immunity.[25] In addition, splenocytes from mice vaccinated with OVA-USMD exhibited faster proliferation (Figure 6H) and a higher level of cytokine interferon IFN-γ secretion (Figure 6I) compared to splenocytes from mice vaccinated with OVA-SC and OVA-IM injection groups after 72 h of culture. Furthermore, the OVA-specific cytotoxic T lymphocyte (CTL) lysis of splenic T lymphocytes from vaccinated mice toward the B16 melanoma cell line transfected with ovalbumin (B16-OVA) depended on the ratio of effector and target cells. In this study, OVA-USMD exhibited a significantly higher lysis efficiency compared to the OVA-SC and OVA-IM injection groups (Figure 6J). Finally, all the major organs looked normal after the application of USMD (Figure S22, Supporting Information). Taken together, these findings suggest that vaccination with OVA-USMD could induce more robust antigen-specific humoral and cellular immune responses when compared to vaccination through SC and IM injections.

2.7. Sterilization of USMD

Sterilization of microneedle products is crucial for preventing infections, ensuring patient safety, and complying with regulations.[26] In this study, we evaluated the compatibility of the USMD with three commonly used sterilization technologies for medical devices: Ethylene oxide (EtO), Electron beam (E-Beam), and γ-ray. Following the guidelines for disinfection and sterilization in healthcare facilities issued by the Centers for Disease Control and Prevention (CDC),[27] the USMD underwent sterilization using EtO (400–600 mg L^{-1}), E-Beam (25 kGy), and γ-ray (25 kGy). Our data demonstrated that EtO sterilization had no impact on the properties of USMD (**Figure 7**A). The sterilized and nonsterilized groups showed no significant differences in swelling ratio and compressive strength after the EtO sterilization process. The swelling ratio and compressive strength were recorded as 3710 ± 133.7% and 63.12 ± 3.6 Mpa, respectively, after sterilization. In contrast, USMD subjected to E-Beam and

Figure 5. Mitigation of imiquimod-induced psoriasis via drug loaded USMD. A) Schematic illustration of USMD for the treatment of imiquimod-induced psoriasis. B) Representative photographs of imiquimod-induced psoriasis mice treated with various treatments. C) PASI scores of psoriatic skin. D) Imiquimod-induced psoriasis mice body weight variation during treatment. E) Spleen weights of imiquimod-induced psoriasis mice at day 7. F) H&E staining of skin tissue sections from mice after the specified treatments. The arrows indicate the thickness of epidermal. Scale bar, 200 μm. G) Quantification of epidermal thickness after the psoriasis therapy in H&E-stained microphotographs. H) Toluidine blue staining of skin tissue sections from mice after the specified treatments. The arrows indicate mast cells. Scale bar, 200 μm. I) Number of mast cells in mice back in toluidine blue stained microphotographs. In (C)–(I), data are presented as mean ± s.d. (n = 5 independent animals). Two-tailed Student's t-test was used to compare the mitigation of imiquimod-induced psoriasis via the MTX-USMD group with other administration routes and the IL-17A USMD group with IL-17A SC group. In (C), ****$P < 0.0001$ versus model, MTX-Oral and MTX-Topical; ****$P < 0.0001$ versus IL-17A SC group. In (E), *$P = 0.0283$ versus MTX-Topical, **$P = 0.0054$ versus MTX-Oral, ****$P < 0.0001$ versus model, IL-17A USMD no significant difference (ns, $P = 0.0764$) versus IL-17A SC group. In (G) and (I), ****$P < 0.0001$ versus model, MTX-Oral and MTX-Topical; ****$P < 0.0001$ versus IL-17A SC group. In (F) and (H), three images were taken with similar results.

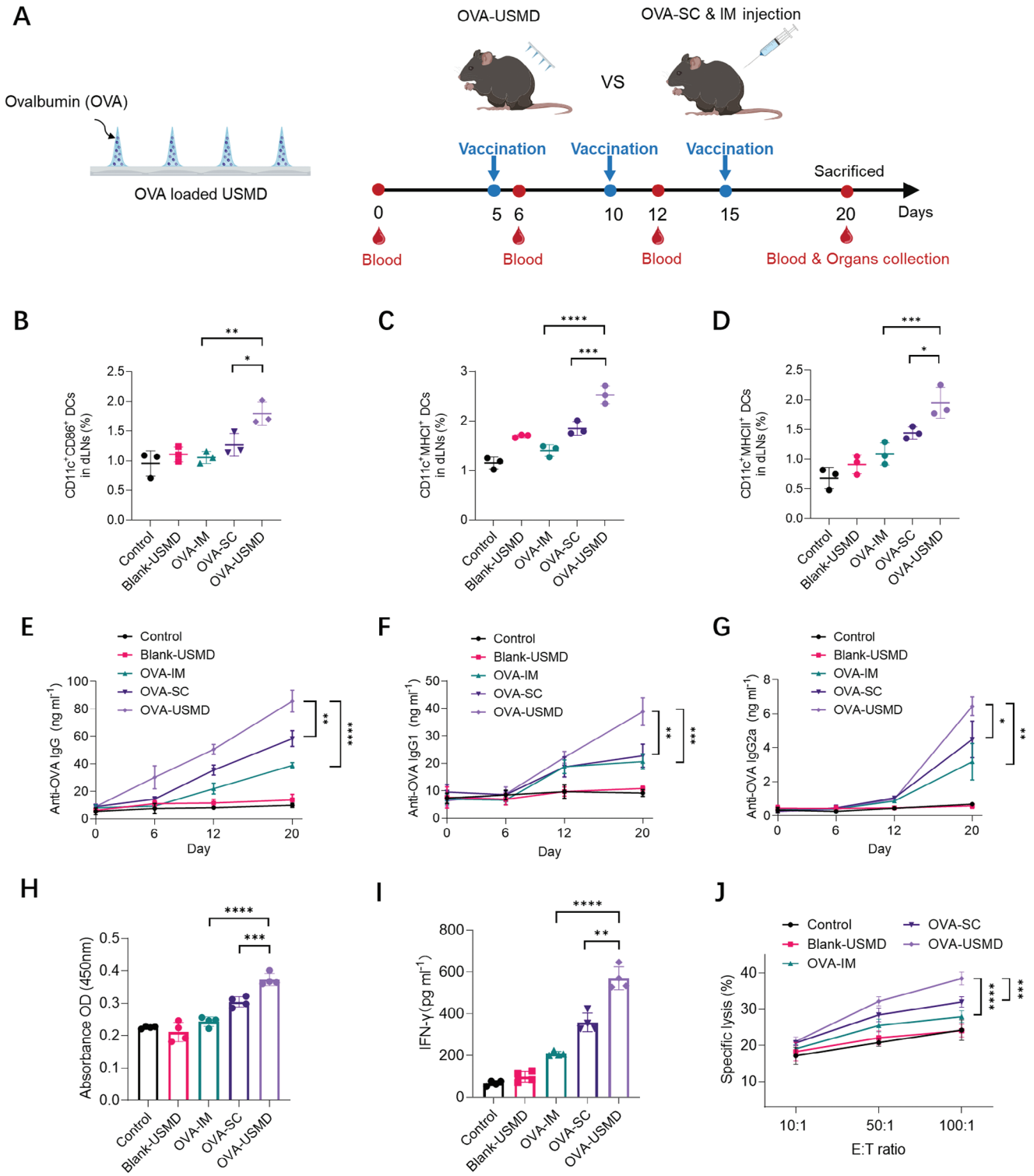

Figure 6. Vaccination by USMD loaded with OVA. A) Schematic illustration of vaccination with OVA-USMD in mice. Vaccination with subcutaneous (OVA-SC) and intramuscular (OVA-IM) injections of OVA were used for comparison. Quantification of the percentage of B) $CD11c^+CD86^+$ DCs, C) $CD11c^+MHCI^+$ DCs, and D) $CD11c^+MHCII^+$ DCs in draining lymph nodes (dLNs) excised from mice in different treatment groups, analyzed by flow cytometry. The levels of E) IgG, F) IgG1, and G) IgG2a in serum were determined by ELISA. H) In vitro proliferation of extracted splenocytes restimulated with 50 μg mL^{-1} antigen (OVA). The absorbance was obtained using a CCK-8 assay. I) Secretion level of IFN-γ in the culture supernatants after 72 h of culture. J) Determination of cytotoxic T lymphocyte (CTL) activity in vitro. Effector cells (splenocytes) and target cells (B16-OVA cells) were cocultured at different ratios. "E:T" refers to the ratio of effector cells E) and target cells T). In (B)–(D), data are presented as mean ± s.d. (n = 3 independent animals). In (E)–(J), data are presented as mean ± s.d. (n = 4 independent animals). Two-tailed Student's t-test was used to compare vaccination with

OVA-USMD with OVA-SC and OVA-IM. In (B), *P = 0.03 versus OVA-SC, **P = 0.0045 versus OVA-IM. In (C), ****P = 0.0068 versus OVA-SC, ***P = 0.0008 OVA-IM. In (D), *P = 0.0351 versus OVA-SC, **P = 0.0098 versus OVA-IM. In (E), **P = 0.0014 versus OVA-SC, ****P < 0.0001 versus OVA-IM. In (F), **P = 0.0027 versus OVA-SC, ***P = 0.0007 versus OVA-IM. In (G), *P = 0.018 versus OVA-SC, **P = 0.0017 versus OVA-IM. In (H), ***P = 0.0015 versus OVA-SC, ****P < 0.0001 versus OVA-IM. In (I), **P = 0.001 versus OVA-SC, ****P < 0.0001 versus OVA-IM. In (J), ***P = 0.0002 versus OVA-SC, ****P < 0.0001 versus OVA-IM.

γ-ray sterilization exhibited a lower swelling ratio but higher mechanical strength (Figure 7B,C; and Figure S23, Supporting Information). This may be due to an increase in the crosslinking degree of USMD caused by the irradiation of E-Beam and γ-ray.[28] These findings suggest that EtO sterilization is a suitable option for sterilizing USMD while preserving its properties.

2.8. Biocompatibility of USMD

To study the biocompatibility of the USMD (Figure S27, Supporting Information), the USMD was pressed into the back skin of mice and removed. After the resin substrate was removed, the tips of USMD were fully embedded under the skin surface and the mice skin gradually recovered 12 h postadministration. H&E staining revealed no obvious inflammatory cell infiltration or pathophysiological response of USMD after 24 h postadministration. Besides, the USMD and the microdosage of Irgacure 1173 used in USMD fabrication not adversely affect the cells. In summary, the USMD demonstrated a satisfactory biocompatibility and biosafety.

3. Discussion

In this study, we introduced a novel transdermal drug delivery strategy called USMD (ultraswelling microneedle device) that enables the convenient loading and transdermal delivery of hydrophilic drugs with varying molecular weights. The USMD has demonstrated significant potential for clinical translation due to several factors, including its simple and scalable fabrication methods, the use of commercially available materials known for their excellent biocompatibility, facile, and efficient drug loading and delivery capabilities, as well as its overall safety profile. One of the notable features of USMD is its capability to load drugs through a diffusion effect when immersed in a drug solution (Figure 1). Additionally, the microneedle array can regain its original shape and mechanical strength, facilitating efficient penetration (Figures 2 and 3). In contrast to the drug loading methods employed in conventional microneedle systems (such as coating or encapsulation within the matrix during fabrication), the drug loading process using USMD does not necessitate any specialized equipment and can be carried out by end users with minimal expertise. Additionally, this drug loading method is a postloading process conducted under mild conditions, which helps avoid the harsh conditions involved in preloading processes that can potentially disrupt or greatly compromise the activity of the loaded drug. Several microneedle systems have been developed for postloading drugs. For example, Liu et al. reported on poly (ethylene glycol) diacrylate (PEGDA) microneedles designed for peptide loading and delivery.[29] In a more recent study, Pitakjakpipop et al. developed zwitterionic polymer microneedles for the postloading of protein drugs.[30] However, these microneedle systems are limited to loading drugs with a molecular weight below 10 kDa. For instance, the peptide used in the first study, Gap 26, has a molecular weight of 1550.78 Da,[29] while the protein drug used in the second study is insulin with a molecular weight of 5807.69 Da.[30] In addition, it takes ≈1 day to perform drug loading using these microneedles, which includes achieving the maximum loading dosage and allowing sufficient

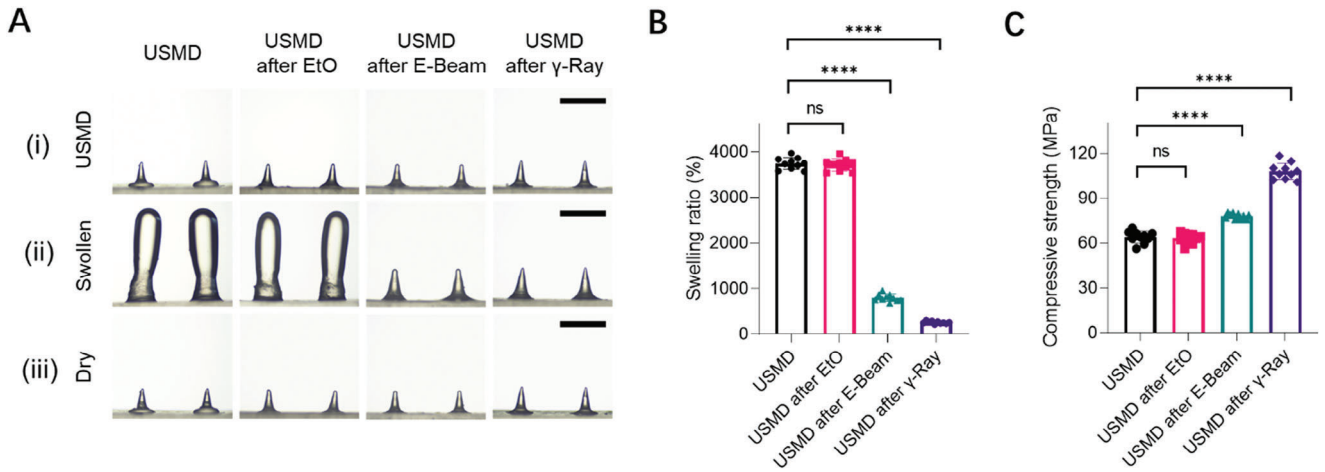

Figure 7. Sterilization of USMD. A) Representative images of USMD before and after EtO, E-Beam, and γ-Ray sterilization. i) USMD. ii) After swelling for 1 min in PBS. iii) After 15 min of drying. Scale bar, 1000 µm. B) Swelling ratio and C) compressive strength of USMD before and after EtO, E-Beam and γ-Ray sterilization. In (A), three images were taken and all experiments were repeated independently three times with similar results. In (B),(C), data are presented as mean ± s.d. (n = 10 independent samples). Two-tailed Student's t-test was used to compare sterilization with USMD after EtO, E-Beam and γ-Ray sterilization. In (B), ns (P = 0.5995) versus USMD after the EtO group, ****P < 0.0001 versus USMD after E-Beam and γ-Ray group. In (C), ns (P = 0.6006) versus USMD after the EtO group, ****P < 0.0001 versus USMD after E-Beam and γ-Ray group.

drying time before application. By contrast, the USMD is capable of loading drugs with a molecular weight of up to 500 kDa due to its rapid and ultraswelling properties. The entire drug loading process can be accomplished under 20 min (refer to Figures S8 and S15, Supporting Information), highlighting its exceptional efficiency and convenience. Furthermore, the microneedle components of USMD can be easily detached from the base substrate under the shear force of the thumb after insertion into skin tissue (Figure 2E,F). This characteristic not only enhances the effectiveness of drug delivery but also minimizes the discomfort typically associated with the long-term retention of the base substrate on skin surface. Additionally, it has the potential to safeguard patients' medication privacy.[8b]

To fabricate the USMD, we introduced a micromolding based method that involved hydrated crosslinking and cryogenic-demolding process. We demonstrated that the hydrated crosslinking and cryogenic-demolding are two critical steps that determine the ultraswelling properties of the USMD. The underlying reason can be explained as follows (refer to Figure S2, Supporting Information). In comparison to dehydrated crosslinking, hydrated crosslinking leads to a looser network of crosslinked polymers due to the presence of water between the polymer chains. This loose polymer network persists even after microneedle drying, allowing for greater swelling compared to microneedles with dehydrated crosslinking. During cryogenic demolding, ice crystals form within the polymer network's pores, further expanding the porous space by elongating the polymer chains. As a result, the combination of hydrated crosslinking and cryogenic demolding enables the hydrogel microneedles of USMD to possess an ultraswelling property. This detailed mechanism warrants further investigation in future studies. We anticipate that this fabrication strategy can be expanded to create dry-hydrogel-based materials for diverse applications requiring ultraswelling functionality, such as drug delivery, wound healing, and soft robotics.[31]

We have demonstrated that the USMD is capable of loading a variety of hydrophilic drugs, ranging from small molecules to large molecules (Figure 3A). The amount of drug loaded in USMD can be regulated by adjusting the drug concentration in the incubation solution (Figure 3B–E). To demonstrate the potential clinical application of USMD, we selected two commercially available drugs for treating psoriasis: MTX and IL-17A antibody. Each of these drugs was loaded into USMD, and their therapeutic efficacy was evaluated after administration. Our findings indicate that the administration of either MTX or IL-17A with USMD results in stronger efficacy in mitigating imiquimod-induced psoriasis compared to their conventional administration methods, including oral and topical delivery of MTX and SC injection of IL-17A (Figure 5). Both MTX and IL-17A are immunoregulatory drugs that specifically target immune cells involved in the inflammatory process.[32][33] The enhanced therapeutic efficacy may be attributed to the abundance of immune cells in the skin,[34] allowing for the direct functioning of MTX and IL-17A when administered via USMD. Another application of USMD is vaccination. Our study demonstrated that the delivery of the model antigen OVA using USMD elicited more robust antigen-specific humoral and cellular immune responses compared to conventional SC and IM injections of OVA (Figure 6). Compared to subcutaneous and muscle tissue, the skin is highly immunoreactive and contains abundant antigen-presenting cells (APCs), including Langerhans cells in the epidermis and dendritic cells (DCs) in the dermis. When administered intradermally using USMD, vaccines can be effectively captured by these APCs. This process enhances various immune activities, such as antigen presentation, T cell priming, and the generation of antibody-secreting plasma cells.[35] Our results align with previous studies that have employed microneedles for vaccine immunization.[36] Further studies will utilize specific vaccines to evaluate the tangible clinical benefits of USMD. Additionally, the administration frequency and dosage of USMD merit further optimization to maximize vaccine-induced immunity.

In addition to its applications in psoriasis treatment and vaccination, the USMD holds promise for various other applications due to its versatility in loading different active molecules. For example, active cosmeceuticals like niacinamide and vitamin C can be incorporated into USMD and utilized for cosmetic purposes such as antiaging and skin whitening.[37] The use of USMD for loading and delivering immune checkpoint blockade (ICB) monoclonal antibodies (mAbs) is anticipated to enhance cancer immunotherapy. Previous studies have demonstrated that intradermal routes of administration lead to significant T cell responses, attributed to the increased accumulation of mAbs within lymph nodes.[38] In addition to transdermal applications, USMD can be applied to target other tissues, including the oral mucosa, the eye, and vascular tissues.[39]

The USMD can be utilized in two ways: it can either be preloaded with drugs by manufacturers and supplied to end-users as a microneedle-based drug-device combination system, or it can be directly provided to end-users as a medical device, allowing them to load the desired drugs for various purposes. The sterilization of medical devices is a crucial step in ensuring their safety and effectiveness, particularly for those that need to be inserted or implanted into the human body.[40] We found that the USMD can withstand EtO sterilization without compromising its swelling ability and mechanical strength (Figure 7). This result highlights the future potential of USMD as a medical device.

The proposed USMD has demonstrated convenience, efficiency, and versatility in drug loading and delivery for different therapeutic applications. There are still some translational considerations for this infant platform. First, the drugs that can be loaded by USMD are restricted to the hydrophilic molecules because the microneedle part of USMD are made from the hydrophilic polymer. In the future, the materials utilized in the production of organogels hold promise for developing the USMD capable of loading and delivering hydrophobic molecules.[41] Second, when compared to conventional syringes, the USMD has a relatively limited capacity for drug loading due to its microscale size. This limitation becomes critical when administering high dosages of drugs that are necessary to achieve potent therapeutic effects. The issue can be addressed by either redesigning the microneedle component with larger dimensions or increasing the number of microneedle arrays. It is recommended to utilize USMD for loading and delivering drugs that can induce robust therapeutic outcomes with minimal dosage requirements. Examples of such drugs include cytokines, vaccines, and hormones. Third, further investigation into the sterilization of USMD is still warranted. We only employed one condition of EtO for sterilizing the USMD. It is important to study the effects of various

parameters (such as gas concentration, humidity, temperature, and time) on the properties of USMD to determine the optimal sterilization conditions, taking into account cost-effectiveness. Fourth, the development of an applicator for USMD is necessary to facilitate user manipulation and penetration. Fifth, for future conversion and application, it is recommended that the USMD be stored in a low-humidity environment after drug loading and be protected from dampness during administration to maintain its mechanical properties. With further development and optimization, we believe this user-friendly and versatile USMD could greatly improve the efficacy and accessibility of transdermal therapies in research institutes, hospitals, and even home settings.

4. Conclusion

In summary, we introduced an ultraswelling microneedle device (USMD) that enables simple and efficient loading and transdermal delivery of hydrophilic drugs with varying molecular weights. By using a special micromolding technique involving hydrated crosslinking and cryogenic-demolding, the microneedle part of USMD has a rapid swelling ratio of ≈3800%, allowing for loading drugs with a molecular weight of up to 500 kDa. The drug loading process using the device just involves incubating the microneedle part in a drug solution for 1 min, followed by a 15 min drying. The microneedle part can easily penetrate into skin under compression and detach from the base substrate under shear as an implantable drug reservoir to release the payload. Transdermal administration of desired therapeutic agents using USMD could significantly surpass conventional administration routes in mitigating psoriasis and enhancing vaccination immunity. The USMD could withstand ethylene oxide sterilization, suggesting its potential as a medical device. Given its simplicity and versatility in both drug loading and administration, this USMD could eventually enhance the accessibility of transdermal therapies in research institutes, hospitals, and even home settings.

5. Experimental Section

Fabrication of USMD: The designed stainless-steel microneedles were utilized as a master mold to replicate the master microneedle structure. Briefly, PDMS (10:1 w/w ratio of pre-polymer base to curing agent) was poured into the master mold, vacuumed in the oven for 10 min, and cured it at 70 °C for 1 h before demolding. Then the obtained PDMS mold was sterilized by ultraviolet exposure before USMD preparation. 100 mg of methacrylylated hyaluronic acid (MeHA) was dissolved in 1 mL of deionized water to form a hydrophilic polymer solution. Next, photo-initiator Irgacure 1173 (0.5 mg mL^{-1}) was added to create a mixed solution. The hydrogel solution was then poured onto the surface of a microneedle mold, and centrifuged at high speed for 3 min. The excess hydrogel solution was removed and biocompatible photocurable resin was added. After curing with ultraviolet light (100.0 mW cm^{-2}, 365 nm), the patch was frozen in a refrigerator (−20 °C) for 4 h, demolded in the above low-temperature environment, and then dried at room environment (25 °C, 40% RH) for 1 h to obtain USMD.

Morphology of USMD: The ultraswelling microneedle device was imaged using various microscopy techniques, including an inverted fluorescence microscope (CKX53, Olympus), a field emission scanning electron microscope (SEM, JSM-IT800), and a digital camera. To modify the drug-loading process of USMD, the USMD with different crosslinking times were soaked in PBS for 1 min, and then dried. The images of different states were captured using a stereo microscope (SZX16, Olympus). Additionally, the swollen state cross-sectional images of USMD after different crosslinking times were obtained using the SEM. Specifically, the USMD were soaked in PBS for 1 min, the cross-section was exposed using medical scissors, and then frozen in liquid nitrogen before undergoing freeze-drying.

Swelling Ability Access of USMD: The swelling ratio of the ultraswelling microneedle device was obtained by comparing its mass before and after incubation in PBS. First, the mass of the USMD (m_1) was recorded. Then, the needles of the USMD were immersed in PBS for 1 min and taken out, the mass was recorded as (m_2). After separating all the needles from the resin, the mass of the resin was recorded as (m_0). The swelling ratio (R) of the USMD was calculated using the following formula

$$\text{Swellingratio}\ (\%) = (m_2 - m_1)/(m_1 - m_0) \times 100 \quad (1)$$

where R is the swelling ratio, m_1 is the mass of the USMD, m_2 is the mass of USMD after swelling, and m_0 is the mass of the resin base substrate.

Mechanical Properties of USMD: The mechanical strength of USMD was examined using an Instron tensile meter (68SC-05, USA). Briefly, the USMD was placed on a flat metal plate and the needles were facing up, and the transducer approached the USMD in the vertical direction at a speed of 0.5 mm min^{-1}. Displacement and force measurements began when the transducer first touched the microneedle tips and continued until the sensor traveled 0.4 mm from the microneedle tips toward the base substrate. Different crosslinking times of USMD were used for comparison. The compressive strength of USMD is calculated by the formula

$$F = P/A \quad (2)$$

Where F is the compressive strength (MPa), P is the maximum load to the USMD (N); A is a cross section of the area of the USMD resisting the load (mm^2).

The shear force of the USMD was measured by attaching the USMD to a flat metal plate positioned vertically, the transducer approached the side of USMD in the vertical direction at a speed of 0.5 mm min^{-1}. Displacement and force measurements began when the transducer first touched the microneedle and continued until the sensor travelled 4.5 mm parallel to the other side of USMD. The USMD without skin insertion, after insertion and remained for 10 and 30 s, respectively, were used for comparison.

Skin Insertion of USMD: To evaluate the penetration, the USMD with different crosslinking times (0.5, 1, 2, 3, and 5 min) were vertically inserted into porcine skin (fresh porcine cadaver skin was purchased from the local supermarket) by thumb press and removed immediately. The skin tissue was further fixed with 4% paraformaldehyde and stained with H&E for histological analysis. The penetration depth was measured by ImageJ software (version 1.53a, no plugin used). To evaluate the separation, USMD loaded with Rho6G were inserted into porcine skin by pressing with a thumb for 30 s, then gently sliding to one side along the skin surface to apply a shear force to separate the microneedles from the base substrate. After separation, the skin containing swollen and separated needles was examined by an inverted fluorescence microscope (CKX53, Olympus) to identify the detached microneedles embedded in the skin. The skin tissue was further fixed with 4% paraformaldehyde and cut into 10 µm sections for histological analysis.

Drug Loading Capacity of USMD: To investigate the drug loading capacity of USMD, different molecules including Rho6G (479 Da), FITC-OVA (40 kDa), FITC-Dex (150 kDa), and FITC-Dex (500 kDa) were loaded into the USMD at initial drug solution concentration ranging from 5 to 20 mg mL^{-1}, using PBS as the solvent. A single USMD patch, consisting of one hundred microneedles, to determine the maximum drug load per needle is employed. The needle of the USMD was immersed in the solution for 1 min, and images were captured using a stereo microscope (SZX16, Olympus) with both bright-field and fluorescence fields. Next, the USMD loaded with different drugs were incubated in PBS containing hyaluronidase (300 U mL^{-1}) until the needle of USMD were completely dissolved, causing the release of the drugs inside. The absorbance of all the drug solutions was measured using a microplate reader (TECAN,

Spark). The concentration of released drug was quantified using calibration curves of each molecule with a known concentration (0–200 μg mL^{-1}), and the amount of each molecule loaded into per needle of USMD was calculated accordingly.

Ex Vivo and In Vivo Drug Release of USMD: The USMD loaded with different molecules including Rho6G (479 Da), FITC-OVA (40 kDa), FITC-Dex (150 kDa), and FITC-Dex (500 kDa) were immersed in PBS and kept at 37 °C. At the predetermined time points, 50 μL of the solution was transferred to a 96-well plate and the absorbance was examined with a microplate reader (TECAN, Spark). 50 μL of fresh PBS was added back to the solution and the concentrations of each drug released at different time points were calculated based on the standard curves, and the cumulative release of drugs were calculated for the different time points for each type of molecule.

To investigate the in vitro diffuse study of USMD, a skin model by coating the 1% w/v agarose hydrogel (mimicking dermis of skin) with a parafilm layer (representing the water impermeable stratum corneum and epidermis) were developed. Four needles of UMSD loaded with FITC-OVA (40 kDa) were inserted in 1% agarose hydrogel. After 30 s, the base substrate was separated. The process of swelling and drug release of USMD were monitored by stereo microscope (SZX16, Olympus) in a fluorescence field at various time points and the images were taken.

The in vivo drug release of ultraswelling microneedle device was conducted by C57BL/6 mice. The mice were dehaired under anesthesia before use. The USMD loaded with FITC-OVA (40 kDa) was applied on the mice back for 30 s and the substrate was removed subsequently. Then the mice were imaged under an in vivo imaging system (IVIS Spectrum, PerkinElmer) at the designated time from day 0 to 7. To quantitatively analyze the fluorescence intensity, the average radiant efficiency (photons s^{-1} cm^{-2} sr^{-1} μW^{-1}) was calculated within specific regions of interest (ROIs) that were placed on the USMD application site. The ROIs value acquired from untreated skin on the same mice was subtracted. Additionally, to enable comparisons across different time points, the data were normalized to the fluorescence intensity measured at day 0.

Imiquimod-Induced Psoriasis Mouse Model and In Vivo Treatment: The study was approved by the Animal Research Ethics Committee of Hangzhou Institute of Medicine (HIM), Chinese Academy of Sciences (2023R0002). The BALB/c mice (8–10 weeks old, 20–25 g) were dehaired under anesthesia and fed normally for 1 day to restore the stratum corneum. Then 100 mg of imiquimod (IMQ) cream was applied on the shaved region of the mice back for seven consecutive days. The mice were separated into eight groups and two treatment timelines: MTX treatment and IL-17A treatment.

For the MTX treatment timeline, the mice were treated three times from day 1 to day 7 with different treatment groups, including: 1) control group (not stimulated by IMQ cream), 2) model group (no treatment), 3) blank-USMD group (USMD without any therapeutic molecule), 4) MTX-oral group (normal saline with 30 μg of MTX), 5) MTX-topical group (MeHA solution with 30 μg of MTX), 6) MTX-USMD group (USMD loaded with 30 μg MTX). For the IL-17A treatment timeline, the mice were treated once on day 1 with different treatment groups: 7) IL-17A SC group (subcutaneous injection of 60 μg IL-17A) and 8) IL-17A USMD group (USMD loaded with 60 μg IL-17A). The quantification of MTX was determined by absorption spectrophotometry using microplate reader, and the quantification of IL-17A was measured using ELISA kits following the protocols provided by the manufacturers (Figure S25, Supporting Information). All treatments were conducted 12 h after the application of IMQ cream. In the USMD group, the patch was pressed firmly for 30 s to achieve penetration and swelling through the stratum corneum and epidermis (Figure S26, Supporting Information). After that, the resin substrate was removed from the back of the mice. During the treatment, the Psoriasis Area and Severity Index (PASI) score was recorded by grading erythema, scaling, and induration as 0 (no symptoms), 1 (mild), 2 (moderate), 3 (severe), or 4 (very severe). On day 7, the mice were sacrificed to obtain skin tissues, livers, and spleens. The level of alanine transaminase (ALT) in the liver was measured using an assay kit according to the manufacturer's protocol. The skin tissue was fixed in 4% paraformaldehyde to preserve the tissue structure, followed by staining with hematoxylin and eosin (H&E) and toluidine blue for microscopic observation.

Vaccination by USMD Loaded with OVA: The experimental procedures involving female C57BL/6 mice (6–8 weeks old, 18–20 g) were conducted in accordance with ethical approval obtained from the Animal Research Ethics Committee of Hangzhou Institute of Medicine (HIM), Chinese Academy of Sciences (2023R0003). The mice were dehaired under anesthesia and fed normally for 1 day to restore the stratum corneum, randomly divided into five treatment groups: 1) control (without any vaccination), 2) blank-USMD (USMD without any vaccine antigen), 3) OVA-IM (intramuscular injection of 100 μg ovalbumin), 4) OVA-SC (subcutaneous injection of 100 μg ovalbumin), 5) OVA-USMD (USMD loaded with 100 μg of ovalbumin, following the loading and quantification method of FITC-OVA). Each group of mice received vaccination on day 5, 10, and 15. Blood samples were collected on day 0, 6, 12, and 20, while lymph nodes and major organs were extracted on day 20. To analyze DC infiltration, activation and maturation, lymph node cells were stained with FITC-conjugated CD11c antibody staining, APC-conjugated CD86 antibody, BV-conjugated MHCI antibody and APC-conjugated MHCII antibody. The stained cells were measured by a flow cytometer (Beckman Coulter, CytoFLEX LX) and were analyzed by FlowJo software (TreeStar, version 10.5.3).

To determine the levels of anti-OVA IgG, IgG1, and IgG2a in serum, the double sandwich ELISA method was used on days 0, 6, 12, and 20. Splenocytes were seeded in a 96-well plate at a density of 5×10^5 cells per well and restimulated with 50 μg mL^{-1} of OVA for 72 h. The proliferation of splenocytes was evaluated using CCK-8 assays following the manufacturer's protocol and the OD value were demined by a microplate reader (excitation: 450 nm). The production of IFN-γ in culture supernatants was measured using a mouse IFN-γ enzyme-linked immunosorbent assay kit. The CTL assay was carried out by loading the B16 melanoma cell line transfected with ovalbumin (B16-OVA; target cells) with a fluorescence enhancing ligand. Effector cells (splenocytes) and target cells (B16-OVA) were cocultured at cell number ratios of 10:1, 50:1, and 100:1. After incubation for 2 h at 37 °C, lysed target cells were quantified. The major organs were cryosectioned and H&E stained to analyze for any organ damage after the vaccination process.

Sterilization of USMD: The EtO sterilization and E-beam irradiation were conducted by Zhejiang Huanyi Sterilization Technology Company (Zhejiang, China). The EtO concentration used for sterilization was controlled from 400 to 600 mg mL^{-1}, and the injection time was 4 h and the temperature maintained at 37–63 °C. The relative humidity was kept between 40% and 80%, and a 12 h hold time was maintained during the sterilization process. E-beam sterilization was conducted by a pulsing transformer at 25 kGy and the sterilization was conducted at ambient temperatures. γ-ray sterilization was conducted by Zhejiang YinDu Radiation Technology Company (Zhejiang, China) using a cobalt-60 irradiator at 25 kGy and the sterilization was conducted at ambient temperature. To ensure the validity of the sterilization process, nonsterilized controls underwent the same transport and storage conditions as the test samples.

Biocompatibility of USMD: The USMD was inserted on the dorsal skin of mice and removed after 30 s. To visualize skin resealing and irritation, the treated sites were imaged with a smartphone at the designated times (0, 6, 12, and 24 h). For histological analysis, the treated skin samples were collected and processed for H&E staining (Sakura, Full-automatic dyeing machine, DRS-Prisma-P-JCS&Film-JC2). Immortalized mouse dendritic cells purchased from MeisenCTCC company (Zhejiang, China) were cultured in RPMI-1640 in an incubator containing 5% CO_2 at 37 °C. After incubating cells in 96-well plates for 24 h, a fresh medium containing USMD or Irgacure 1173 (0.5 mg mL^{-1}) was added. After another 24 h of incubation, the CCK-8 kit was utilized to detect the cell viability according to the manufacturer's protocol.

Statistical Analysis: All experiments used biological replicates that consisted of cells in nonrepeated, independent cell culture wells or tissue samples from different animals, unless specified otherwise. Quantitative data are represented as mean ± s.d. Statistical analysis was performed by using two-tailed Student's *t*-test or original one-way ANOVA. $P < 0.05$ were considered statistically significant ($^*P < 0.05$, $^{**}P < 0.01$,

$^{***}P < 0.001$, $^{****}P < 0.0001$). GraphPad Prism 8.3 was used for data analysis. Excel 2019 was used for calculating the exact P value when $P < 0.0001$.

Supporting Information

Supporting Information is available from the Wiley Online Library or from the author.

Acknowledgements

F.L.Q. acknowledged the financial support from the National Key Research and Development Program of China (No. 2021YFA0910103). H.C. acknowledged the financial support from the National Natural Science Foundation of China (No. 82202329), startup funding (No. 2021QD08-1: 2021QD08-2) supported by the Hangzhou Institute of Medicine (HIM), Chinese Academy of Sciences, and a research grant from Medcraft Biotech. Inc. (No. 2022HX01).

Conflict of Interest

Z.M.L. and H.C. are inventors of two patents that have been applied based on the data in this manuscript. H.C. is the scientific founder of a company that develops microneedles. Rest authors have no conflict of interest in this work.

Author Contributions

Z.M.L. and H.C. are inventors of two patents that have been applied based on the data in this manuscript. H.C. is the scientific founder of a company that develops microneedles.

Data Availability Statement

The data that support the findings of this study are available from the corresponding author upon reasonable request.

Keywords

cryogenic-demolding, drug delivery, medical devices, microneedles, ultra-swelling

Received: July 26, 2023
Revised: September 26, 2023
Published online:

[1] M. R. Prausnitz, R. Langer, *Nat. Biotechnol.* **2008**, *26*, 1261.
[2] a) B. Winblad, J. C. Machado, *Expert Opin. Drug Delivery* **2008**, *5*, 1377; b) J. Shao, J. Zhang, N. A. Villasis, X. Li, G. Chen, G. Chen, J. Yu, Y. Zhang, J. Wang, Y. Gao, J. Lin, P. Huang, Z. Gu, *Matter* **2023**, *6*, 158; c) M. Higaki, M. Kameyama, M. Udagawa, Y. Ueno, Y. Yamaguchi, R. Igarashi, T. Ishihara, Y. Mizushima, *Diabetes Technol. Ther.* **2006**, *8*, 369.
[3] V. Phatale, K. K. Vaiphei, S. Jha, D. Patil, M. Agrawal, A. Alexander, *J. Controlled Release* **2022**, *351*, 361.
[4] S. M. Bal, Z. Ding, E. Van Riet, W. Jiskoot, J. A. Bouwstra, *J. Controlled Release* **2010**, *148*, 266.
[5] a) L. Yan, M. Alba, N. Tabassum, N. H. Voelcker, *Adv. Therap.* **2019**, *2*, 1900141; b) M. R. Prausnitz, S. Mitragotri, R. Langer, *Nat. Rev. Drug Discovery* **2004**, *3*, 115.
[6] P. Karande, A. Jain, K. Ergun, V. Kispersky, S. Mitragotri, *Proc. Natl. Acad. Sci. USA* **2005**, *102*, 4688.
[7] R. Yang, T. Wei, H. Goldberg, W. Wang, K. Cullion, D. S. Kohane, *Adv. Mater.* **2017**, *29*, 1606596.
[8] a) H. Chang, S. W. T. Chew, M. Zheng, D. C. S. Lio, C. Wiraja, Y. Mei, X. Ning, M. Cui, A. Than, P. Shi, D. Wang, K. Pu, P. Chen, H. Liu, C. Xu, *Nat. Biomed. Eng.* **2021**, *5*, 1008; b) W. Li, R. N. Terry, J. Tang, M. R. Feng, S. P. Schwendeman, M. R. Prausnitz, *Nat. Biomed. Eng.* **2019**, *3*, 220; c) J. Yu, J. Wang, Y. Zhang, G. Chen, W. Mao, Y. Ye, A. R. Kahkoska, J. B. Buse, R. Langer, Z. Gu, *Nat. Biomed. Eng.* **2020**, *4*, 499; d) S. P. Sullivan, D. G. Koutsonanos, M. Del Pilar Martin, J. W. Lee, V. Zarnitsyn, S.-O. Choi, N. Murthy, R. W. Compans, I. Skountzou, M. R. Prausnitz, *Nat. Med.* **2010**, *16*, 915; e) P. C. Demuth, Y. Min, B. Huang, J. A. Kramer, A. D. Miller, D. H. Barouch, P. T. Hammond, D. J. Irvine, *Nat. Mater.* **2013**, *12*, 367.
[9] T. Sheng, B. Luo, W. Zhang, X. Ge, J. Yu, Y. Zhang, Z. Gu, *Adv. Drug Delivery Rev.* **2021**, *179*, 113919.
[10] a) T. Bauleth-Ramos, N. El-Sayed, F. Fontana, M. Lobita, M.-A. Shahbazi, H. A. Santos, *Mater. Today* **2023**, *63*, 239; b) A. H. Sabri, Y. Kim, M. Marlow, D. J. Scurr, J. Segal, A. K. Banga, L. Kagan, J. B. Lee, *Adv. Drug Delivery Rev.* **2020**, *153*, 195; c) B. Mbituyimana, G. Ma, Z. Shi, G. Yang, *Biomater. Adv.* **2022**, *142*, 213151.
[11] N. G. Kotla, I. L. Mohd Isa, A. Larrañaga, B. Maddiboyina, S. K. Swamy, G. Sivaraman, P. K. Vemula, *Adv. Healthcare Mater.* **2023**, *12*, e2203104.
[12] H. Chang, M. Zheng, X. Yu, A. Than, R. Z. Seeni, R. Kang, J. Tian, D. P. Khanh, L. Liu, P. Chen, C. Xu, *Adv. Mater.* **2017**, *29*, 1702243.
[13] J. Zhu, X. Zhou, H.-J. Kim, M. Qu, X. Jiang, K. Lee, L. Ren, Q. Wu, C. Wang, X. Zhu, P. Tebon, S. Zhang, J. Lee, N. Ashammakhi, S. Ahadian, M. R. Dokmeci, Z. Gu, W. Sun, A. Khademhosseini, *Small* **2020**, *16*, e1905910.
[14] E. Abd, S. A. Yousef, M. N. Pastore, K. Telaprolu, Y. H. Mohammed, S. Namjoshi, J. E. Grice, M. S. Roberts, *Clin. Pharmacol.* **2016**, *8*, 163.
[15] S. Bao, B. Silverstein, *Ergonomics* **2005**, *48*, 288.
[16] Y. Luo, K. R. Kirker, G. D. Prestwich, *J. Controlled Release* **2000**, *69*, 169.
[17] H. Chang, M. Zheng, X. Yu, A. Than, R. Z. Seeni, R. Kang, J. Tian, D. P. Khanh, L. Liu, P. Chen, C. Xu, *Adv. Mater.* **2017**, *29*, 1702243.
[18] A. W. Armstrong, C. Read, *JAMA, J. Am. Med. Assoc.* **2020**, *323*, 1945.
[19] a) I. B. Mcinnes, P. J. Mease, B. Kirkham, A. Kavanaugh, C. T. Ritchlin, P. Rahman, D. Van Der Heijde, R. Landewé, P. G. Conaghan, A. B. Gottlieb, H. Richards, L. Pricop, G. Ligozio, M. Patekar, S. Mpofu, *Lancet* **2015**, *386*, 1137; b) L. Fala, *Am. Health Drug Benefits* **2016**, *9*, 60.
[20] M. Jabeen, A.-S. Boisgard, A. Danoy, N. El Kholti, J.-P. Salvi, R. Boulieu, B. Fromy, B. Verrier, M. Lamrayah, *Pharmaceutics* **2020**, *12*, 789.
[21] I. Dolz-Pérez, M. A. Sallam, E. Masiá, D. Morelló-Bolumar, M. D. Pérez Del Caz, P. Graff, D. Abdelmonsif, S. Hedtrich, V. J. Nebot, M. J. Vicent, *J. Controlled Release* **2020**, *318*, 210.
[22] Q. Li, W. Liu, S. Gao, Y. Mao, Y. Xin, *BMC Immunol.* **2021**, *22*, 11.
[23] W. Y. Jiang, A. D. Chattedee, S. P. Raychaudhuri, S. K. Raychaudhuri, E. M. Farber, *Int. J. Dermatol.* **2001**, *40*, 699.
[24] T. C. Theoharides, K.-D. Alysandratos, A. Angelidou, D.-A. Delivanis, N. Sismanopoulos, B. Zhang, S. Asadi, M. Vasiadi, Z. Weng, A. Miniati, D. Kalogeromitros, *Biochim. Biophys. Acta* **2012**, *1822*, 21.
[25] F. Belardelli, *APMIS* **1995**, *103*, 161.
[26] M. Dul, M. Alali, M. Ameri, M. D. Burke, C. M. Craig, B. P. Creelman, L. Dick, R. F. Donnelly, M. N. Eakins, C. Frivold, A. H. Forster, P.-A. Gilbert, S. Henke, S. Henry, D. Hunt, H. Lewis, H. I. Maibach, J. J. Mistilis, J.-H. Park, M. R. Prausnitz, D. K. Robinson, C. A. R. Hernandez, C. Ross, J. Shin, T. J. Speaker, K. M. Taylor, D. Zehrung,

J. C. Birchall, C. Jarrahian, S. A. Coulman, *J. Controlled Release* **2023**, *361*, 236.
[27] W. A. Rutala, D. J. Weber, Guideline for disinfection and sterilization in healthcare facilities, **2008**, https://stacks.cdc.gov/view/cdc/11560 (accessed: 2008).
[28] M. Demeter, I. Calina, A. Scari?Oreanu, M. Micutz, *Gels* **2022**, *8*, 27.
[29] S. Liu, D. C. Yeo, C. Wiraja, H. L. Tey, M. Mrksich, C. Xu, *Bioeng. Transl. Med.* **2017**, *2*, 258.
[30] H. Pitakjakpipop, R. Rajan, K. Tantisantisom, P. Opaprakasit, D. D. Nguyen, V. A. Ho, K. Matsumura, P. Khanchaitit, *Biomacromolecules* **2022**, *23*, 365.
[31] a) Y. Lee, W. J. Song, J.-Y. Sun, *Mater. Today Phys.* **2020**, *15*, 100258; b) M. J. Zohuriaan-Mehr, A. Pourjavadi, H. Salimi, M. Kurdtabar, *Polym. Advan. Technol.* **2009**, *20*, 655.
[32] A. Blauvelt, A. Chiricozzi, *Clin. Rev. Allergy Immunol.* **2018**, *55*, 379.
[33] M. Priyadarssini, L. Chandrashekar, M. Rajappa, *Clin. Exp. Dermatol.* **2019**, *44*, 491.
[34] F. O. Nestle, P. Di Meglio, J.-Z. Qin, B. J. Nickoloff, *Nat. Rev. Immunol.* **2009**, *9*, 679.
[35] Z. Zhao, A. Ukidve, A. Dasgupta, S. Mitragotri, *Adv. Drug Delivery Rev.* **2018**, *127*, 3.
[36] a) C. Caudill, J. L. Perry, K. Iliadis, A. T. Tessema, B. J. Lee, B. S. Mecham, S. Tian, J. M. Desimone, *Proc. Natl. Acad. Sci. USA* **2021**, *118*, e2102595118; b) G. Kang, M. Kim, H. Yang, J. Shin, J. Sim, H. Ahn, M. Jang, Y. Kim, H. S. Min, H. Jung, *Adv. Funct. Mater.* **2023**, *33*, 2210805.
[37] C.-C. Yu, A. Shah, N. Amiri, C. Marcus, M. O. G. Nayeem, A. K. Bhayadia, A. Karami, C. Dagdeviren, *Adv. Mater.* **2023**, *35*, 2300066.
[38] D. M. Francis, M. P. Manspeaker, A. Schudel, L. F. Sestito, M. J. O'melia, H. T. Kissick, B. P. Pollack, E. K. Waller, S. N. Thomas, *Sci. Transl. Med.* **2020**, *12*, eaay3575.
[39] A. Panda, V. A. Matadh, S. Suresh, H. N. Shivakumar, S. N. Murthy, *Drug Delivery Transl. Res.* **2022**, *12*, 67.
[40] W. A. Rutala, D. J. Weber, *Infect. Control. Hosp. Epidemiol.* **2007**, *28*, 146.
[41] M. A. Kuzina, D. D. Kartsev, A. V. Stratonovich, P. A. Levkin, *Adv. Funct. Mater.* **2023**, *33*, 2301421.